Theor Chim Acta (1994) 88: 447–472

Theoretica Chimica Acta

Relativistic and electron correlation effects on the *d-d* spectrum of transition metal fluorides

L. Visscher and W. C. Nieuwpoort

Laboratory of Chemical Physics and Material Science Centre, Nijenborgh 4, NL-9747 AG Groningen, The Netherlands. Email: Luuk @CHEM.RUG.NL. Fax: (31) 50634200

Received December 13, 1993/Accepted March 31, 1994

Summary. The electronic spectra of the transition metal complexes CoF_6^{2-}, RhF_6^{2-} and IrF_6^{2-} that occur in the solids Cs_2MeF_6 are calculated. Hartree–Fock and Dirac–Fock calculations followed by non-relativistic and relativistic CI calculations respectively are used to study the influence of relativity and electron correlation. The calculated transitions are found to agree fairly well with experiment, the largest discrepancies arising from the neglect of differential dynamical electron correlation effects.

Key words: Hartree–Fock – Dirac method – Relativistic configuration interaction – Transition metal fluorides

1 Introduction

Ab initio computational methods based on the non-relativistic Schrödinger equation are nowadays applied quite routinely to describe the electronic structure of 3*d* and 4*d* transition metal complexes. In such calculatons the main problem is to give an accurate description of the large electron–electron correlation that is present in partly filled *d*-shells. The most conspicuous errors that arise from the use of a non-relativistic theory instead of a relativistic theory are caused by the neglect of spin–orbit coupling. This deficiency can, however, in most cases be accounted for by the use of a perturbative spin–orbit operator.

In 5*d* transition metal complexes relativity leads to significant changes in the electronic wave functions compared to non-relativistically calculated wave functions. In these systems relativistic corrections are no longer small and the use of perturbation theory based on non-relativistically determined wave functions is more difficult. Methods that use non-relativistically determined orbitals as a one-electron basis for (approximate) relativistic configuration interaction (CI) calculations may need larger expansions to converge than methods that include relativity from the outset.

In this work such a more rigorous approach is followed by employing a relativistic formalism throughout. The basic equation that we use is the Dirac–Coulomb–Gaunt equation that implicitly includes all one-electron relativistic effects and the magnetic (Gaunt) correction to the Coulomb two-electron

interaction. We use the Dirac–Fock approach to obtain four-component spinors that are used to set up a determinantal CI space for subsequent relativistic CI calculations. We can thus treat relativity and electron correlation on an equal footing and study the influence and interplay of both on the electronic spectra.

This method has previously been applied to closed shell group IV hydrides [1], a lanthanide complex [2] and recently to the PtH molecule [3]. We now study the properties of the MeF_6^{2-} complex ions of cobalt, rhodium and iridium as representative examples of transition metal complexes across the periodic table. These ions were chosen because experimental data (structures and electronic spectra) of all three ions are available. Since the metal ions belong to the same column of the periodic table, they have the same valence electron configurations which simplifies the comparison of the results.

2 Theory

We have performed various types of CI calculations using a determinantal basis built from the 4-component spinors obtained from DHF calculations. Below a short resumé of the DHF method and CI method is given. Unless otherwise stated all calculations have been performed using the MOLFDIR program package [4].

2.1 The DHF method

The starting point of our calculations is the Dirac–Coulomb equation

$$H\Psi = E\Psi, \tag{1}$$

$$H = \sum_{i}^{N} h_i + \sum_{i<j} g_{ij}, \tag{2}$$

where h is the one-electron Dirac hamiltonian

$$h = \begin{bmatrix} V \cdot I_2 & c(\sigma \cdot p) \\ c(\sigma \cdot p) & (V - 2c^2) \cdot I_2 \end{bmatrix}, \tag{3}$$

I_2 and σ are the 2×2 identity and Pauli matrices respectively, while the potential V describes the interaction of the electrons with the fixed nuclear framework. A detailed description of this hamiltonian may be found is standard textbooks [5, 6]. The electron–electron interaction, g_{ij}, is given by the Coulomb operator

$$g_{ij} = \frac{1}{r_{ij}} \tag{4}$$

and represents in this context the 0th order approximation of the full relativistic electron-electron interaction. A first order correction is provided by the Breit operator [7], which may be split [8] into a magnetic part, usually termed the Gaunt interaction [9], and a retardation part.

$$g_{ij}^{\text{Breit}} = -\frac{(\alpha_i \cdot \alpha_j)}{r_{ij}} - \frac{(\alpha_i \cdot \nabla_i)(\alpha_j \cdot \nabla_j)}{2} = g_{ij}^{\text{Gaunt}} + g_{ij}^{\text{retardation}}. \tag{5}$$

Our computer program allows for the inclusion of the Gaunt interaction either in a variational or in a perturbative scheme.

From the Dirac–Coulomb equation open-shell DHF equations can be derived in the same way as the non-relativistic Hartree–Fock equations [10]. By minimising the (averaged) energy expression of a system with one open shell, we get the following set of equations

$$F^{C}=h+Q^{C}+Q^{O}+\alpha L^{O}, \qquad F^{O}=h+Q^{C}+aQ^{O}+\alpha L^{C}, \tag{6}$$

$$Q^{C}=\sum_{k} J_k-K_k, \qquad Q^{O}=f\sum_{m} J_m-K_m, \tag{7}$$

$$L^{C}=\sum_{k} L_k, \qquad L^{O}=f\sum_{m} L_m, \tag{8}$$

$$J_i|j\rangle=\langle i|g_{12}|i\rangle|j\rangle, \qquad K_i|j\rangle=\langle i|g_{12}|j\rangle|i\rangle, \tag{9}$$

$$L_i|j\rangle=\langle i|Q^{O}|j\rangle|i\rangle+\langle i|j\rangle Q^{O}|i\rangle. \tag{10}$$

In these equations k and m are used to label closed and open shell molecular 4-spinors respectively. The fractional occupation number (f) of the open shell spinors and the coupling coefficients (a and α) are defined by the number of open shell electrons (n) and the number of open shell spinors (m)

$$f=\frac{n}{m}, \qquad a=\frac{m(n-1)}{n(m-1)}, \qquad \alpha=\frac{1-a}{1-f}. \tag{11}$$

The DHF equations are expanded in a Gaussian type basis set. This basis sets is made up of two subsets describing the upper (large) components and the lower (small) components of the spinors. In order to get a correct representation of all operators these basses are chosen to be related by the kinetic or atomic balance relation [11]. For open shell systems the average of configuration energy is minimised after which the energies of individual states can be obtained by complete open shell configuration interaction (COSCI) [2] – diagonalisation of the CI-matrix of all possible configurations in the open shell manifold.

2.2 The relativistic CI method

We have developed a relativistic version of the restricted active space configuration interaction (RASCI) [12] method which can be used to improve the wave functions and energy differences found in the DHF (-COSCI) step.

To describe the method it is convenient to write the Dirac–Coulomb–(Gaunt) hamiltonian in second quantised form. Using the generators of the unitary group $E_{ij}=a_i+a_j$ the hamiltonian can be written as

$$H=\sum_{i,j}\langle i|h|j\rangle E_{ij}+\frac{1}{2}\sum_{i,j,k,l}(ij|g|kl)(E_{ij}E_{kl}-E_{il}\delta_{jk}). \tag{12}$$

In this equation molecular spinors are labelled by i, j, k and l. The summation is restricted to the electron solutions, since we neglect any (virtual) positron–electron pair creation. We expand the many-electron wave functions in the determinantal basis $\{\Phi_I\}$ defined above. The result is a matrix representation of the hamiltonian which can be expressed as a sum of 1- and 2-electron integrals multiplied by

coupling constants γ_{ij}^{IJ} and Γ_{ijkl}^{IJ}, respectively.

$$H_{IJ}=\sum_{i,j} h_{ij}\gamma_{ij}^{IJ}+\frac{1}{2}\sum_{i,j,k,l}(ij|kl)\Gamma_{ijkl}^{IJ}, \tag{13}$$

with $h_{ij}=\langle i|h|j\rangle$, $(ij|kl)=(ij|g|kl)$, $\gamma_{ij}^{IJ}=\langle I|E_{ij}|J\rangle$ and $\Gamma_{ijkl}^{IJ}=\frac{1}{2}\langle I|E_{ij}E_{kl}-E_{il}\,\delta_{kj}|J\rangle$.

Since the matrix in general will be too large to hold in memory, we use the direct diagonalisation technique to Davidson [13] to find the desired roots. The main difference with non-relativistic direct CI methods is that the number of relativistic integrals is about 2^4 times as large since each molecular orbital corresponds to two molecular spinors. Another complication is that the integrals in general will be complex since the hamiltonian contains complex operators. Thus the number of virtual spinors and the number of determinants that can be used is smaller than what is presently possible with efficient non-relativistic CI methods. Our direct RASCI code can at present handle expansions up to about 200,000 determinants using an active spinor space of about 100 spinors.

In the RASCI formalism the spinor set is first divided in a core set, an active set and an external or deleted set, after which the active set is further subdivided into three sets (RAS1, RAS2, RAS3). By specifying a minimum number of electrons that has to reside in RAS1 spinors and a maximum number of electrons that may be excited to the RAS3 space, most conventional types of CI spaces can be defined.

In the case of the MeF_6^{2-} ions the RAS1 set consists of the 36 fluorine 2*p*-like spinors, the RAS2 set consists of the 10 open Me *nd*-like spinors, and the RAS3 set is formed by the 46 virtual spinors with lowest spinor energies. Note that in this formalism the COSCI calculation mentioned earlier corresponds to a calculation solely in the RAS2 space, the RAS1 and RAS3 spinors being constrained to have occupations of one and zero respectively.

In the present application the COSCI method is equivalent to the well known Ligand Field CI (LFCI) method in which all $t_{2g}^x e_g^y$ configurations with $x+y=5$, the number of *d*-electrons, are taken into account. Complete diagonalisation of this small CI space is possible and gives a set of intermediary coupled wave functions and a first estimate of the *dd*-spectrum.

The LFCI space is subsequently extended into a Charge Transfer CI (CTCI) reference space by allowing single, double, triple, or higher excitations from RAS1 to RAS2. These excitations mix (low-lying) charge-transfer (Me^{3+}, Me^{2+}, Me^{+}) states into the LFCI wave functions. The CTCI method is intended to treat the non-dynamical correlation or near degeneracy effects that may arise from the low-lying charge-transfer states. Formally the method provides for a properly dissociating wavefunction as well. Finally we must account for the fact that the calculations are based on one set of *d*-like spinors obtained in the DHF calculation for the average energy of all d^5 related open shell states. This set will not be optimal for the states with higher *d*-occupancy that arise in constructing the CTCI space. This deficiency may in first order be corrected by extending the CTCI space to include all single excitations out of the valence spinors of the CT states into the available virtual spinors. This approach has been succesfully applied before in non-relativistic calculations on transition metal compounds [14, 15] and has been called, for obvious reasons, relaxed charge transfer (RCT) or first order (FO) CI method.

In the present application the treatment of dynamical correlation by means of inclusion of double excitations into the RAS3 space is prohibited by the large size of the active space.

3 Basis sets

Gaussian type basis sets were optimised to minimise the energy of the Me^{4+} d^5 configurational average. Because no relativistic basis set optimisation program is available at present, we used the non-relativistic code ASCF [16] for this purpose. During the optimisation process the *d*-exponents were constrained to be a subset of the *s*-exponents. The advantage of applying these constraints on the *d*-exponents is that the primitive basis for the small component *p*-functions, as obtained by kinetic balance, is already contained in the small component functions that arise from the large component *s*-functions. The *f*-exponents were similarly constrained to be a subset of the *p*-exponents, to keep the number of small component *d*-functions as low as possible.

The non-relativistic exponent optimisation gives quite reasonable results apart from a deficiency in the basis for the $p_{1/2}$ spinors which lacks some steep basis functions. This deficiency was remedied by adding one extra tight *p* function to the Rh basis and two extra to the Ir basis. The exponents were determined by logarithmic extrapolation of the original set of exponents.

Using these sets of primitive gaussians the atomic spinors of the Me^{4+} ions were determined after which general contracted bases were formed consisting of all occupied spinors (1*s*, 2*s*, 2*p*, 3*s*, 3*p* 3*d*). The valence region is described at triple-zeta level by keeping two outer *s*-functions, one outer *p*-function and two outer *d*-functions uncontracted and by adding extra *s*, *p*, *d* and *f* diffuse functions. The uncontracted functions were kinetically balanced, the contracted functions that were obtained from the occupied spinors were atomically balanced.

To describe the fluorine ions we used Wachters [17] primitive fluorine basis. The general contraction was based on a calculation on the F^- closed shell ion and the resulting triple-zeta valence basis was extended with 1 *d* polarisation function.

The size of the basis sets is given in Table 1. The primitive basis sets of all ions are given in Appendix 1. Contraction coefficients are available upon request.

Table 1. Basis set sizes

Co	(17*s*, 10*p*, 7*d*, 1*f*;	nrel.	[6*s*, 4*p*, 4*d*, 1*f*]
	10*s*, 17*p*, 10*d*, 7*f*, 1*g*)	rel.	[6*s*, 5*p*, 4*d*, 1*f*; 5*s*, 9*p*, 7*d*, 5*f*, 1*g*]
Rh	(18*s*, 14*p*, 11*d*, 1*f*;	nrel	[7*s*, 5*p*, 5*d*, 1*f*]
	14*s*, 18*p*, 14*d*, 11*f*, 1*g*)	rel.	[7*s*, 8*p*, 7*d*, 1*f*; 5*s*, 12*p*, 9*d*, 7*f*, 1*g*]
Ir	(21*s*, 15*p*, 13*d*, 7*f*;	nrel.	[8*s*, 6*p*, 6*d*, 2*f*]
	15*s*, 21*p*, 15*d*, 13*d*, 7*g*)	rel.	[8*s*, 10*p*, 9*d*, 3*f*; 6*s*, 14*p*, 12*d*, 9*f*, 3*g*]
F	(10*s*, 6*p*, 1*d*; 6*s*, 10*p*, 6*d*, 1*f*)	nrel.	[5*s*, 4*p*, 1*d*]
		rel.	[5*s*, 4*p*, 1*d*; 4*s*, 5*p*, 4*d*, 1*f*]

4 Atomic calculations

To investigate the quality of the basis sets we have compared the differences between the absolute energies at Hartree–Fock and at Dirac–Fock level calculated respectively with the contracted basis sets and numerically with the program GRASP [18]. The basis set Hartree–Fock calculations were done with the non-relativistic option of our program package MOLFDIR, the numerical Hartree–Fock limit was obtained using a value of *c*, the speed of light, that was scaled by a factor of 10,000.

Table 2. Energy differences (eV) between numerical and basis set Dirac–Fock calculations on the d^n averages ($n=5,6,7$). $\Delta E = E$ (Basis set)-E(Numerical)

	Non-relativistic			Relativistic		
	Co	Rh	Ir	Co	Rh	Ir
$\Delta E(Me^{4+})$	0.22	0.56	2.98	0.44	1.79	32.27
$\Delta E(Me^{3+})$	0.26	0.54	3.00	0.47	1.78	32.28
$\Delta E(Me^{2+})$	0.39	0.53	3.05	0.61	1.76	32.32

Table 3. Energy differences (eV) between numerical and basis set COSCI calculations of the (relative) $Me^{4+}d^5$ energies

	Non-relativistic			Relativistic		
	Co	Rh	Ir	Co	Rh	Ir
Weighted average error	0.007	0.013	0.004	0.008	0.009	0.002
Maximum error	0.013	0.026	0.008	0.015	0.018	0.005

The weak singularity of the relativistic wavefunction at the nucleus formally disappears if one uses a finite nuclear model. Stil, the lack of very steep functions to describe the $1s_{1/2}$ and $2p_{1/2}$ spinors in the vicinity of the nucleus causes an absolute error in the relativistic energies that is much larger than the absolute error in the non-relativistic energies. The energy differences between the different valence configurations are, however, quite satisfactory and accurate to about 0.2 eV (Table 2). To study the effect of basis set errors on the d–d spectrum we have performed COSCI calculations based both on the numerical spinor set and on the basis set spinor set. If we compare the relative energies of the states in the d^5 manifold we find that the differences between both calculations are small: maximally 26 meV (Table 3).

In the optimisation of the Rh^{4+} energy two s- (and therefore also two d-functions) ended up with almost the same exponential parameter (0.4435 and 0.3888). Such a close spacing is not very efficient and may give numerical inaccuracies in the molecular calculations. We therefore substituted for the latter primitive function a function with exponent 0.1803 (obtained by logaritmic extrapolation). This explains the somewhat larger deviations from the numerical results in the Rh^{4+} spectrum (Table 3).

The tables show that the basis sets give a good description of the different oxidation states of the metal ions, but they do not test the validity of the COSCI approach to calculate accurate spectra. Comparison with experimental data is desirable but is hampered by the scarcity of spectral data for the higher oxidation states of the metal ions. Excitation energies for the 4+ ions are only available for cobalt [19]. Comparison with the Me^{2+} electronic spectrum is possible for both cobalt and rhodium [20] (Table 4).

The relativistic COSCI method gives a good description of the intramultiplet spin–orbit splittings, except for the very small splitting of the ^4G excited state of

Table 4. Relativistic COSCI spectrum of the Co^{4+}, Co^{2+} and Rh^{2+} free ions. Energies (eV) given relative to the ground state. Intramultiplet splittings (meV) are given in parenthesis

State	Co^{4+}		State	Co^{2+}		Rh^{2+}	
	Exp. [19]	COSCI		Exp. [20]	COSCI	Exp. [20]	COSCI
$^6S_{5/2}$	0.00	0.00	$^4F_{9/2}$	0.00 (0)	0.00 (0)	0.00 (0)	0.00 (0)
$^4G_{11/2}$	4.61 (0)	5.21 (0)	$^4F_{7/2}$	0.10 (104)	0.10 (103)	0.27 (266)	0.26 (256)
$^4G_{9/2}$	4.62 (9)	5.21 (−1)	$^4F_{5/2}$	0.18 (180)	0.17 (179)	0.43 (432)	0.42 (424)
$^4G_{7/2}$	4.62 (9)	5.20 (−14)	$^4F_{3/2}$	0.23 (231)	0.23 (232)	0.54 (536)	0.53 (532)
$^4G_{5/2}$	4.63 (11)	5.21 (6)	$^4P_{3/2}$	1.88 (0)	2.41 (0)	1.36 (0)	1.85 (0)
$^4P_{3/2}$	5.05 (0)	5.99 (0)	$^4P_{5/2}$	1.91 (28)	2.44 (32)	1.37 (8)	1.85 (−2)
$^4P_{5/2}$	5.07 (17)	6.00 (16)	$^4P_{1/2}$	1.96 (76)	2.48 (78)	1.55 (183)	2.02 (170)
$^4P_{1/2}$	5.09 (34)	6.02 (36)	$^2G_{9/2}$	2.11 (0)	2.40 (0)	1.74 (0)	1.91 (0)
$^4D_{7/2}$	5.54 (0)	6.48 (0)	$^2G_{7/2}$	2.20 (98)	2.50 (99)	1.89 (150)	2.17 (256)
$^4D_{1/2}$	5.57 (25)	6.49 (14)	$^2H_{11/2}$	2.82 (0)	3.20 (0)	2.42 (0)	2.54 (0)
$^4D_{5/2}$	5.58 (34)	6.51 (35)	$^2H_{9/2}$	2.91 (89)	3.28 (82)	2.73 (250)	2.79 (250)
$^4D_{3/2}$	5.58 (34)	6.51 (30)					
$^2I_{11/2}$	6.74 (0)	7.42 (0)					
$^2I_{13/2}$	6.74 (5)	7.44 (16)					

Co^{4+} where it reverses the order of the states. Note, however, that the main feature of d^5 multiplets, virtually vanishing spin–orbit splittings [21], is reproduced correctly. The method does not deal very well with the intermultiplet splittings. This failure is understandable because at the COSCI level dynamical correlation effects are not accounted for. We may expect the same kind of errors in the molecular calculations.

5 Cluster calculations

5.1 Introduction

In an ionic model we can describe transitional metal complexes as metal cations that are coordinated by ligand anions. In the complexes studied here we find fourfold oxidised metal ions with the configurations [Ar]$3d^5$, [Kr]$4d^5$ and [Xe]$5d^5$ for Co^{4+}, Rh^{4+} and Ir^{4+} respectively. They are octahedrally coordinated by six fluorine anions. The lowest transitions in the electronic spectra of the complexes originate from excitations within the d^5 manifold of the metal ion. The influence of the surrounding ions can in such an approach be accounted for by an electric field of O_h symmetry that lifts the degeneracy of the metal d-orbitals. Many features of the electronic spectra can then be explained on basis of the symmetry of the field [22]. An assumption that is usually made in crystal field theory is that the radial character of the open shell d-like orbitals remains the same. With this assumption the spectrum may be fitted by the use of only a few parameters ($10Dq$, the Racah two-electron parameters B and C and optionally a spin-orbit parameter ζ). This simple model can be refined by accounting for the radial difference between e_g and t_{2g} orbitals but this adds seven more parameters which is in most cases impractical considering the available experimental data.

The unrealistic high formal charge of the metal ions treated here gives, however, rise to difficulties with the interpretation of the electronic structure of the

complexes in a simple ionic model. Covalency will delocalise the ligand electrons and reduce the high formal charge to a more realistic value. In a molecular orbital picture the bonding and anti-bonding combinations of orbitals that are formed from the fluorine *p*-functions and the metal *d*-functions in the t_{2g} and e_g representations give rise to charge transfer that makes the metal ion less positive and the fluorines less negative. In contrast to the electrostatic crystal field picture derived from the ionic model, the formation of covalent bonds can now be considered to be the main source of the perturbing field, which led to the development of ligand field theory. The covalent bonding will also introduce radial differences between the e_g and t_{2g} open shell orbitals since they contribute to a different type of bonding (σ and π respectively). These differences are again not taken into account, however, so that the parametrisation given above is maintained. Interestingly, it has been shown in earlier *ab initio* calculations of *d–d* transitions in iron fluorides and cyanides that, even when the differences are accounted for, the calculated energy levels can be fitted well in this parametrisation [23].

A discussion of the validity of the underlying ideas from an *ab initio* point of view is given by Vanquickenborne et al. [24]. In *ab initio* calculations like the ones presented here, the orbital differences are of course accounted for since the orbitals are determined variationally. This means that the interpretation of the parameters of the ligand field model changes and direct comparison with experimentally derived parameters is difficult. In the relativistic calculations the situation is even more complicated. We now also have to consider the change in character of the orbitals under the influence of spin–orbit coupling. We will therefore in general follow a straightforward approach and compare the observed and calculated transitions directly. In some cases use of a crystal or ligand field model is, however, helpful for a qualitative analysis of the obtained results.

5.2 Symmetry and configurations

The five *d*-orbitals of the central ion are divided in two representations (e_g and t_{2g}) in the octahedral (O_h) point group. The eighteen fluorine *p*-orbitals span a number of representations including e_g and t_{2g} (Table 5).

In the relativistic calculations we will work with one-electron spinors. These functions span the "extra" representations of the full rotational (O(3)*) or the octahedral (O_h^*) double group. For the free ions we find that the *d*-shell is split into a $d_{3/2}$ and $d_{5/2}$ subshell while the fluorine *p*-shells are split into $p_{1/2}$ and $p_{3/2}$ subshells.

The $d_{3/2}$ spinors span the u_g' representation of O_h^* while the $d_{5/2}$ shell is split over its e_g'' and u_g' representations. These representations are of course also spanned if we reverse the construction of molecular double group functions and make

Table 5. Orbitals and spinors in different symmetry groups

	O(3)	O(3)*	O_h	O_h^*
Central ion	*d*	$d_{3/2}$, $d_{5/2}$	e_g, t_{2g}	e_g'', $2u_g'$
Ligands	6*p*	$6p_{1/2}$, $6p_{3/2}$	a_{1g}, e_g, t_{1g}, t_{2g}, $2t_{1u}$, t_{2u}	$2e_g'$, e_g'', $3u_g'$, $2e_u'$, e_u'', $3u_u'$

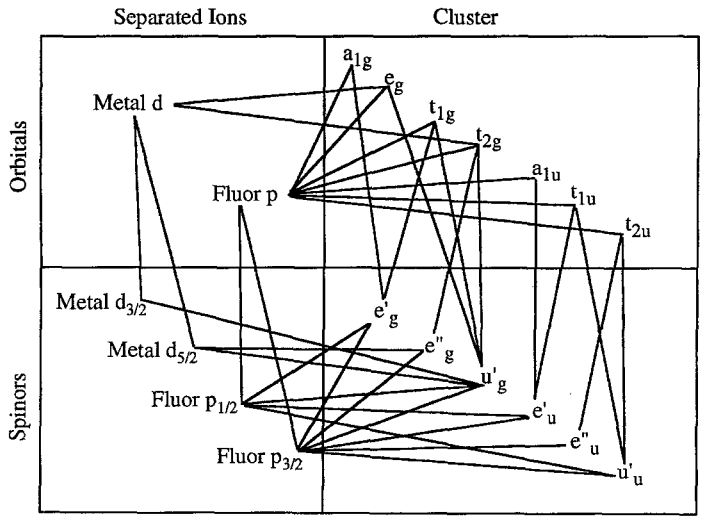

Fig. 1. Relations between orbitals and spinors in different symmetry groups

spinors as products of the e_g and t_{2g} orbitals with α or β spin. We then see that the spinorbitals constructed from the e_g orbitals span the u'_g representation, while the spinorbitals constructed from the t_{2g} orbitals span both the u'_g and the e''_g representation.

In Fig. 1 the relations between the different (spin)orbitals are given. In following discussions on the nature of the spinors and of the splittings we will sometimes loosely speak of t_{2g} (or e_g) *spinors*. This should be read as: "The set of spinors that can be formed from combinations of the e_g (or t_{2g}) *orbitals* multiplied with an α or β spin function".

5.3 Computational details

The splitting of the *d*-shell into 2 or 3 groups of spinors gives various ways of dividing the 5*d* electrons over the different representations. Optimising the energy of all states arising from the possible configurations by separate SCF calculations is in principle possible but impractical. Different spinor sets for all different states would result, implying separate 4-index integral transformations for all states in subsequent CI calculations, which would increase the computational effort considerably. The interpretations of such results would furthermore be more cumbersome because of the differences in spinor sets. Fortunately these complications can be avoided.

Our goal is to obtain one set of spinors that gives a reasonable description of all states. The CI calculations are done (simultaneously) in this molecular spinor basis for all states. To get a balanced description of all states we optimise our spinors for the weighted average energy expression of all configurations that can be made by distributing five electrons over the ten spinors that span the twofold degenerate e''_g and the two four-fold degenerate u'_g representations. This averaged energy expression is equivalent to the non-relativistic weighted average energy expression of the $(t_{2g})^{5-x}\,(e_g)^x$ $(x=0, 1, \ldots, 4)$ configurations.

To check the sensitivity of the results to the choice of the spinor set we have done some non-relativistic calculations on the $^2T_{2g}$ state of CoF_6^{2-}. We studied the energy differences introduced by the use of different one-electon spinor sets for wave functions of different quality. We compare the set of spinors obtained by minimising the energy average of the d^5 configuration (set 1) with the set obtained by minimising the $(t_{2g}{}^5)^2T_{2g}$ energy expression separately (set 2). Since the t_{2g}^5 configuration has a small weight in the total average and the e_g spinors are not optimised at all, these calculations are representative for the maximum differences one may expect from the use of different spinor sets for different states.

In Table 6 we see that the influence of the spinor set diminishes as the level of CI increases. This can be explained by noting that the most important differences between the two spinor sets can be written as rotations between the closed and open shell t_{2g} (and e_g) spinors. In the CTCI calculations excitations from closed to open shell spinors are allowed, hence the differences between the results obtained with the two spinor sets get much smaller. The influence of the use of average spinors on the final results is probably smaller than 0.1 eV since the other states will also have a non-zero, negative, relaxation energy.

Besides the use of one set of spinors for all states we had to use two other approximations to make the calculations feasible.

The first concerns the level of excitation that is allowed in the charge transfer and first order CI calculations. The maximum excitation level for charge transfer excitations (ligand *p* and to metal *d*) is five, giving wave functions with a filled *d*-shell and five holes on the ligands. The weights of such configurations in the CTCI or FOCI wave function are likely to be small since the excitation energies involved are of the order of 3–5 eV per excitation level. This assumption was studied by calculating (non-relativistically) the convergence of the correlation energy of CoF_6^{2-} with an increasing level of excitation in the Charge Transfer CI (Table 7). We see that beyond the triple excitation level no significant changes in

Table 6. $^2T_{2g}$ energy expectation values calculated non-relativistically with different spinor sets and CI spaces. The uncontracted basis without Co f and fluorine *d* functions was used

Wave functions	*E* (Set 1) (a.u.)	*E* (Set 2) (a.u.)	Difference (eV)
Single determinant	−1992.0945	−1992.1166	−0.60
LFCI	−1992.1105	−1992.1291	−0.51
CTCI	−1992.2005	−1992.2051	−0.13

Table 7. Contributions to CoF_6^{2-} CTCI correlation energies (eV) with increasing level of of excitation. The uncontracted basis without Co f and fluorine d functions was used

State	Correlation	Singles	Doubles	Triples	Quadruples
$^2T_{2g}$	−2.45	−0.63	−1.37	−0.44	−0.01
$^4T_{1g}$	−2.11	−0.42	−1.36	−0.33	−0.01
$^4T_{2g}$	−2.36	−0.50	−1.49	−0.36	−0.01
$^6A_{1g}$	−1.17	−0.16	−0.80	−0.21	−0.01

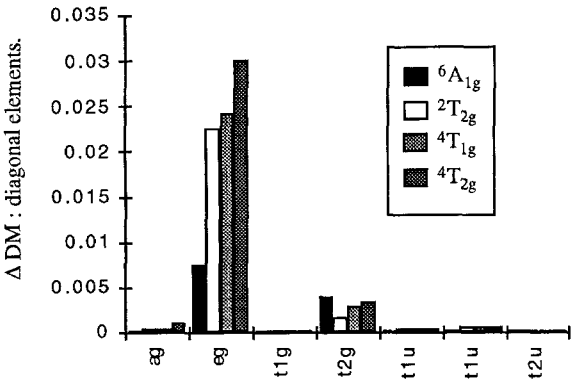

Fig. 2. Diagonal elements of the differential (COSCI-LFCI) density matrices. CoF_6^{2-} at the non-relativistic level

Table 8. Correlation energies (eV) of CoF_6^{2-} with different RAS1 spaces. Note that the figures cannot be compared to Table 7, because different basis sets are used

State	All fluorine p's	e_g and t_{2g}	Difference
$^2T_{2g}$	−1.67	−1.54	0.13
$^4T_{1g}$	−1.49	−1.38	0.12
$^4T_{2g}$	−1.74	−1.53	0.21
$^6A_{1g}$	−0.76	−0.71	0.05

the spectrum occur. We also performed CTCI calculations that allowed triple excitations for RhF_6^{2-} and IrF_6^{2-} but found these to be insignificant (contribution to the correlation energies smaller than 0.03 eV, differences in the spectra smaller than 0.008 eV). In the subsequent calculations we have limited the excitation level in the CTCI and FOCI to doubles.

A second approximation was necessary to make the FOCI calculations computationally possible. Complete first order relaxation of the CTCI wavefunctions asks for a RAS3 space including all virtual (electron) spinors. This would lead to a determinantal space of more than 10^8 determinants, a few orders of magnitude larger than is presently feasible. We therefore restricted our RAS1 and RAS3 space to virtual spinors of e_g and t_{2g} type, since relaxation of the bonding and antibonding spinors in this representations is likely to be the most important. Relaxation of the remaining fluorine *p*-spinors is neglected.

The effect of restricting the RAS1 space to the subset of t_{2g} e_g spinors on the CTCI results was studied by comparing the density matrices from the LFCI and CTCI calculations in the full RAS1 space (Fig. 2). The figure shows that the dominant excitations do indeed involve the e_g and t_{2g} spinors. Comparison of the CTCI results in the full RAS1 (36 fluorine *p*-like) spinors with the results in the restricted basis (14 fluorine *p*-like) spinors confirms this observation as the latter calculation recovers most of the correlation energy at this level (Table 8).

The final expansion space that was used in the CI calculations consisted of 14 fluorine *p*-like spinors in RAS1, 10 Metal *d*-like spinors in RAS2 and 24 virtual spinors. This yielded a number of 13,482 determinants in the CTCI calculations and a number of 562,464 determinants in the FOCI calculation. By the use of

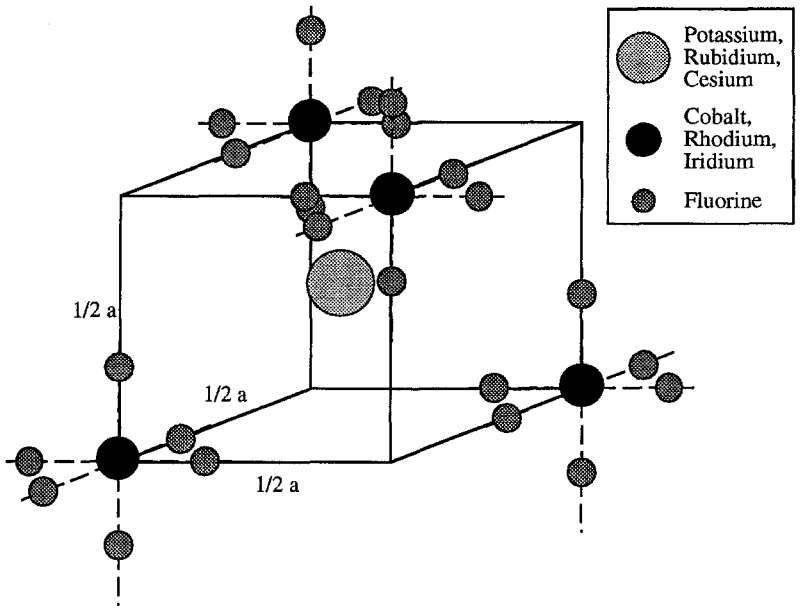

Fig. 3. Cs_2MF_6 lattice. Plotted is part of a unit cell, extended to show the octahedral surrounding of the transition metal. Drawing is not to scale

abelian point group symmetry it was possible to reduce these spaces to subspaces of at most 3,526 (CTCI) and 140,626 (FOCI) determinants.

5.4 Crystal surroundings and cluster geometry

The MeF_6^{2-} ions of cobalt, rhodium and iridium crystallise with a number of alkali cations to form perovskite structures. The compounds have a K_2PtCl_6 like structure in which the MeF_6^{2-} units are separated from each other by about 3.5 Å. The other ions are found at distances slightly larger than 3 Å from the fluorine ions (Fig. 3).

Most experimental spectra available [25, 26, 27] concern the cesium compounds and are rather poorly resolved. In the case of IrF_6^{2-} more precise values for some transitions were obtained by Magnetic Circular Dichroism (MCD) experiments on Cs_2GeF_6, doped with Cs_2IrF_6 [28].

To incorporate the effect of the surrounding ions on the spectra, we have described the surroundings of the IrF_6^{2-} cluster by fitting the Madelung potential of the host (after subtraction of the cluster contributions) to a number of point charges. This fitted potential was also used in the RhF_6^{2-} calculations since no precise value of the lattice parameter (a) of Cs_2RhF_6 was available. In the CoF_6^{2-} calculations we fitted the cluster corrected Madelung potential of the Cs_2CoF_6 lattice.

Both potentials vary slowly over the cluster (Table 9) and lower the spinor energies but do not dramatically influence the spectrum. Calculations on the bare clusters give spectra that differed by less than 0.2 eV from spectra calculated with

Table 9. Potential at lattice sites (Volts)

Position	Cs_2CoF_6	Cs_2GeF_6
Metal sites	9.25	9.00
Fluorine sites	8.81	8.51
Difference	0.44	0.48

the embedded cluster. Other than electrostatic effects from the surroundings are assumed to be small and are not taken into account.

The fit charges and the accuracy of the fits can be found in Appendix 2.

The Me–F distance is not a fixed fraction of the basic lattice parameter (*a*). So knowledge of this lattice parameter alone is not enough to determine the distances within the MeF_6^{2-} ion. Of the three compounds studied only the Cs_2CoF_6 structure is completely determined experimentally. The Co-F distance was estimated to be 1.73 ($\pm$0.05) Å on the basis of X-ray crystallographic data [29]. Of the other two compounds only the Cs–Me distances are known. Recently, however, EXAFS data of the K_2RhF_6 and K_2IrF_6 crystals [30, 31] were published that give precise values for the Rh–F and Ir–F distance in these compounds. This distance is found to be 1.93 Å for both Rh–F and Ir–F. Since we did not have these values at the start-up of our calculations we also determined the distances by a geometry optimisation based on a 3 point parabolic fit of LFCI data (Table 10). These optimisations were carried out for clusters embedded in potentials as described above. As optimum distance we took the equilibrium distance of the lowest $^2T_{2g}$ (E_g'') state.

For CoF_6^{2-} the optimisation procedure gives a distance of 1.76 Å, which is within the (wide) error range of the experimental distance. Miyoshi and Kashiwagi [32] have done non-relativistic SCF calculations on CoF_6^{2-} ground state using embedded and bare cluster models. Using the bare cluster model they found a distance of 1.79 Å. With their most sophisticated model (which included the effect of the first two layers of surrounding ions as point charges) they found a distance of 1.77 Å. These data show that the potential energy curve is almost entirely determined by the intra-molecular interaction with the isolated CoF_6^{2-} complex and is not influenced much by the surrounding ions.

The independence of the Me–F equilibrium distance on the surrounding ions implies that the optimisation process should give values close to Rh–F and Ir–F distances in K_2RhF_6 and K_2IrF_6. Comparing the calculated values in table 10 with the experimental values we find differences of 0.02 Å. This is indeed the same order of accuracy as was obtained for the Co–F distance. However, the calculated Rh–F distance is shorter than the measured distance, while the calculated Ir–F distance is larger than the measured distance. This indicates that the 2 pm accuracy reached by simple LFCI geometry optimisations is somewhat fortuitous and may be less in other compounds.

In the calculations presented in the next section we have used the experimental metal-fluorine distances of 1.730 Å, 1.934 Å and 1.928 Å for cobalt, rhodium and iridium respectively.

5.5 Analysis of the spinor set

To get insight in the amount of covalency that is present in the complexes we have analysed the individual valence e_g and t_{2g} spinors by means of the Mulliken

Table 10. Bond lenghts (picometers) calculated at the LFCI level

State	CoF_6^{2-}			RhF_6^{2-}			IrF_6^{2-}		
	Non-relat.	Relat.	Dif.	Non-relat.	Relat.	Dif.	Non-relat.	Relat.	Dif.
$^2T_{2g}(E''_g)$	177	176	−0.3	191	191	−0.6	196	195	−1.4
$^2T_{2g}(U'_g)$		176	−0.2		190	−0.7		194	−1.6
$^4T_{1g}(U'_g)$	179	179	−0.1	195	194	−0.9	201	198	−3.0
$^4T_{1g}(E''_g)$		179	0.1		194	−1.0		198	−2.8
$^4T_{1g}(U'_g)$		179	0.0		194	−0.8		198	−3.4
$^4T_{1g}(E'_g)$		179	−0.1		194	−0.8		198	−3.4
$^4T_{2g}(E'_g)$	179	179	−0.2	195	195	−0.5	201	198	−3.5
$^4T_{2g}(U'_g)$		179	−0.2		195	−0.5		198	−3.2
$^4T_{2g}(U'_g)$		179	−0.1		195	−0.4		198	−3.3
$^4T_{2g}(E''_g)$		179	−0.2		195	−0.4		198	−3.5
$^4A_{1g}(U'_g)$	181	181	−0.1	198	199	1.0	205	200	−5.6
$^6A_{1g}(E''_g)$		181	−0.1		199	1.0		200	−5.5
Exp. [29–31]		173 (5)			193.4 (0.2)			192.8 (2)	

population analysis scheme [33]. Since we used the same average of configuration energy expression to optimise spinors for the clusters as for the bare metal ions, we can also compare the calculated spinor energies to study trends in the spin–orbit splitting. The shifts that are found in the open shell spinor energies, going from Co to Ir, reflect the shifts found in the Me^{4+} bare ions.

From the population analysis (Table 11) it is clear that the e_g orbitals show more metal-fluorine mixing than the t_{2g} orbitals. This confirms the stronger covalency of the e_g orbitals due to their capacity of forming σ-bonds. The open and closed shell populations are almost complementary which supports the molecular orbital picture that is used in the Ligand Field model. The differences between the

Table 11. Energies and Mulliken population analysis. **a** The highest closed shell e_g (u'_g) spinors. **b** The open shell e_g (u'_g) spinors. **c** The highest closed shell t_{2g}(e''_g, u'_g) spinors. **d** The open shell t_{2g} (e''_g, u'_g) spinors. **e** Mulliken charges of the atoms in the complexes

e_g (closed)	E (eV)	% Me (*d*)	% F (*s*)	% F (*p*)
CoF_6^{2-} (NR)	−19.04	28.2	2.9	70.0
CoF_6^{2-} (R)	−18.93	27.6	2.8	69.6
RhF_6^{2-} (NR)	−18.40	26.6	2.4	70.9
RhF_6^{2-} (R)	−18.24	25.2	2.3	72.1
IrF_6^{2-} (NR)	−18.44	23.6	2.8	73.5
IrF_6^{2-} (R)	−18.06	21.7	2.5	75.7

Table 11b.

e_g (open)	E (eV)	% Me (*d*)	% F (*s*)	% F (*p*)
CoF_6^{2-} (NR)	−18.26	74.3	0.6	25.1
CoF_6^{2-} (R)	−18.14	75.0	0.6	24.4
RhF_6^{2-} (NR)	−12.10	73.0	0.3	27.0
RhF_6^{2-} (R)	−11.74	74.3	0.3	25.7
IrF_6^{2-} (NR)	−9.09	74.6	−0.3	25.6
IrF_6^{2-} (R)	−7.98	77.8	−0.5	22.5

Table 11c.

t_{2g} (closed)	E (eV)	% Me (*d*)	% F (*p*)	% F (*d*)
CoF_6^{2-} (NR)	−17.44	10.7	88.5	0.8
CoF_6^{2-} (R, e''_g)	−17.37	10.3	88.9	0.8
CoF_6^{2-} (R, u'_g)	−17.42	10.4	88.8	0.8
RhF_6^{2-} (NR)	−16.88	13.9	85.3	0.8
RhF_6^{2-} (R, e''_g)	−16.76	12.8	86.4	0.7
RhF_6^{2-} (R, u'_g)	−16.83	13.1	86.2	0.8
IrF_6^{2-} (NR)	−17.01	14.4	84.6	1.0
IrF_6^{2-} (R, e''_g)	−16.76	10.9	88.1	1.0
IrF_6^{2-} (R, u'_g)	−16.87	11.8	87.2	1.0

Table 11d.

t_{2g} (open)	E (eV)	% Me (*d*)	% F (*p*)	% F (*d*)
CoF_6^{2-} (NR)	−21.98	90.9	8.9	0.2
CoF_6^{2-} (R, e_g'')	−21.73	91.2	8.6	0.2
CoF_6^{2-} (R, u_g')	−21.86	91.1	8.7	0.2
RhF_6^{2-} (NR)	−15.84	87.2	12.4	0.4
RhF_6^{2-} (R, e_g'')	−15.30	88.3	11.2	0.5
RhF_6^{2-} (R, u_g')	−15.57	87.8	11.7	0.4
IrF_6^{2-} (NR)	−13.40	86.0	13.9	0.2
IrF_6^{2-} (R, e_g'')	−11.87	89.0	10.6	0.4
IrF_6^{2-} (R, u_g')	−12.69	87.4	12.3	0.3

Table 11e.

	Charge Me	Charge F
CoF_6^{2-} (NR)	2.21	−0.70
CoF_6^{2-} (R)	2.20	−0.70
RhF_6^{2-} (NR)	2.36	−0.73
RhF_6^{2-} (R)	2.37	−0.73
IrF_6^{2-} (NR)	2.81	−0.80
IrF_6^{2-} (R)	2.77	−0.79

different compounds are too small to permit interpretation in terms of changes in covalency.

The differences between the relativistic and the non-relativistic results may be explained by considering the symmetry aspects of the bonding. In the relativistic case there are two representations in which metal-fluorine *d*–*p* bonds may be formed. The u_g' representation is spanned twice by the metal d-functions which means that different combinations can be formed depending on the strength of the spin–orbit coupling.

In the case of weak spin–orbit coupling and strong bonding the u_g' spinors will be combined into e_g and t_{2g} spinors and thus into σ and π-bonds as in the non-relativistic case. Alternatively, in the case of a strong spin–orbit coupling at the central atom and weak bonding, the functions will tend to localise and resemble the atomic double group functions. The open shell u_g' spinors will now be combined to form the $d_{3/2}$ and four of the $d_{5/2}$ spinors. The e_g'' representation then contains the remaining two $d_{5/2}$ spinors.

In other words: the construction of strong σ-bonds is accompanied by a relativistic hybridisation energy that depends on the spin–orbit splitting of the *d*-shell. From the spinor energies of Table 11 we can see that the first case applies here. The relativistic treatment splits the open shell t_{2g} spinors into two groups but this splitting is much smaller than the t_{2g}–e_g splitting. If we compare this splitting with the splitting within the *d*-shell in the Me^{4+} ions, we find that the atomic splitting is reduced to 54% in CoF_6^{2-}, 52% in RhF_6^{2-} and 54% in IrF_6^{2-}. The figures are close to the value of 60% that is obtained if pure t_{2g} metal *d*-combinations are formed.

The decrease relative to this theoretical value can be compared with the results of a simple crystal field model to give information on the covalency of the compounds. If we assume that the open shell orbitals consist of metal *d*-functions only and that both the crystal field and the spin–orbit interaction can be parametrised, we obtain the following matrix equation [34] for the spinor energies

$$\begin{pmatrix} -4Dq+\zeta_d & 0 & 0 \\ 0 & -4Dq-\frac{1}{2}\zeta_d & \sqrt{3/2}\,\zeta_d \\ 0 & \sqrt{3/2}\,\zeta_d & 6Dq \end{pmatrix} \begin{pmatrix} \psi_{(e_g'', t_{2g})} \\ \psi_{(u_g', t_{2g})} \\ \psi_{(u_g', e_g)} \end{pmatrix} = \varepsilon \begin{pmatrix} \psi_{(e_g'', t_{2g})} \\ \psi_{(u_g', t_{2g})} \\ \psi_{(u_g', e_g)} \end{pmatrix}, \tag{14}$$

$\frac{5}{2}\zeta_d$ is the atomic spin–orbit splitting ($\varepsilon_{5/2}-\varepsilon_{3/2}$), while Dq can be obtained from the average energies of the sub configurations (see below). Upon diagonalising this matrix we find values of 62, 64 and 68% of the atomic spin–orbit splitting for Co, Rh and Ir, respectively. The discrepancy with the values found above is due to the delocalisation of the *d*-electrons. The open shell spinors are partly spread out over the fluorines, where a much smaller spin–orbit splitting ($\zeta_{2p}=0.05$ eV) is found. This delocalisation effect counteracts the increase of the percentage of the atomic splitting that would be expected from the increasing strength of the spin–orbit coupling. Since the actual percentages remain fairly constant one can see that there is stronger participation of the *d*'s in the bonding in the iridium complex than in the cobalt and rhodium complexes.

The trend of increasing *d*-participation in the bonding is not directly reflected by the Mulliken charges of the complexes (Table 11e). In such an analysis IrF_6^{2-} is found as the most ionic compound. This is mainly due to changes in the metal *s*- and *p*-occupations of the complexes.

5.6 Configuration interaction

The spinor sets presented above are used for various types of CI calculations that were described above. In addition we have done some calculations on the specific configurations to $t_{2g}^{5-x}e^x$ ($x=0, 1, \ldots, 4$). A theoretical value for the crystal field parameter $10Dq$ was determined by the formula $10Dq=(E(t_{2g}^5)-E(t_{2g}^1e_g^4))/4$ (Table 12)

Table 12. Average energies (eV) for the $t_{2g}^{5-x}e^x(x=0, 1, \ldots, 4)$ configurations, relative to the t_{2g}^5 average energy

	CoF_6^{2-}		RhF_6^{2-}		IrF_6^{2-}	
	Non-rel.	Rel.	Non-rel.	Rel.	Non-rel.	Rel.
t_{2g}^5	0.00	0.00	0.00	0.00	0.00	0.00
$t_{2g}4e_g^1$	2.05	2.06	2.93	2.96	3.76	3.93
$t_{2g}3e_g^2$	4.64	4.65	6.16	6.21	7.74	8.08
$t_{2g}2e_g^3$	7.77	7.76	9.67	9.75	11.95	12.45
$t_{2g}1e_g^4$	11.44	11.40	13.48	13.57	16.38	17.03
$10Dq$	2.86	2.85	3.37	3.39	4.10	4.26
$10Dq$ (Experimental)	2.52		2.54		3.04	

The calculated values for $10Dq$ can be compared with experimental fits and show a rather large discrepancy. This may (partly) be explained by the invalidity of the simple crystal field model in covalent ions. The experimental fit has been done on assignments of states from the lower two configurations, since these are the only states that can be identified. The other transitions lie at higher energies where the much more intense charge transfer type excitations occur that obscure the weak (parity forbidden) d–d transitions. Among the observed transitions at low energy there is none that can be written in terms of only $10Dq$. One always needs to fit the other ligand field parameters B and C as well. In this fit the ratio between B and C is usually fixed which means that a spectrum that in principle would need 12 parameters (the 10 Griffith parameters, $10Dq$ and ζ) is fitted with three free parameters. Calculation of B and C from our results gave rather different results depending on the energy-differences that were fitted. In CoF_6^{2-} for instance, the ratio C/B varied from 4.7 to 6.0 while in the experimental fit a value of 4.9 was taken.

In order to calculate the splittings between the individual states one has to account for the configurational mixing within the d-shell. This mixing is included in all (LF, CT, FO) CI calculations that we have done.

In Tables 13 a–c the results of these CI calculations are presented. We used the Coulomb operator to represent the two-electron interaction, except in the second series of LFCI ($C+G$) calculations in which the Coulomb–Gaunt operator was used. The column NR+SO gives the results of a non-relativistic calculation in which the spin–orbit coupling was accounted for in an approximate way (see below). In the other non-relativistic columns we have shifted the energies of the states by ζ_d. This allows for a better comparison with the experimental and relativistic figures where the zero-point of energy is the $^2T_{2g}$ (E_g'') state instead of the weighted average of $^2T_{2g}$ (E_g'') and $^2T_{2g}$ (U_g').

The energy lowerings (Table 14) and the thereby induced changes in the spectrum that are found upon increasing the level of CI are most prominent for the CoF_6^{2-} complex. A multiconfigurational description is essential here, in order to obtain a correct representation of the lowest states. In IrF_6^{2-} the dominant changes occur if we go from a description without spin–orbit coupling to one were this effect is included. The lowest states can thus be described by a simple LFCI wave function, provided that the spin-orbit coupling is accounted for.

The calculated states of all three compounds can be described within an L–S coupling scheme. The spin–orbit splitting of the lowest doublet and quartet states in IrF_6^{2-} is considerable but remains smaller than the inter-multiplet distances. The relativistic treatment lowers the doublet state relative to the quartet and sextet states. This is caused by interaction between the e_g and the t_{2g} (u_g') spinors. The spin–orbit coupling pushes these two levels apart and thus lowers the energy of the t_{2g}^5 configuration relative to the $t_{2g}^{5-x}e_g^x$ ($x \neq 0$) configurations.

The latter effect can also be modelled with a perturbative ligand field model for the spin–orbit coupling. In this model we assume that the spin–orbit coupling matrix elements between the $^2T_{2g}$, $^4T_{1g}$, $^4T_{2g}$ and $^6A_{1g}$ can be expressed in terms of the atomic spin–orbit parameter ζ_d. This spin–orbit parameter is obtained from a relativistical calculation on Me^{4+} by the relation $\zeta_d = 0.4\ (\varepsilon(d_{3/2}) - \varepsilon(d_{5/2}))$ with ε the Dirac–Fock spinor energy. We add this spin–orbit coupling matrix[35] to the diagonal matrix given by the LFCI energies of these states and rediagonalise. The results show good agreement with our relativistic LFCI results of CoF_6^{2-} and RhF_6^{2-}. The influence of the spin–orbit coupling is overestimated, because covalency effects were neglected in this model. In this simple model we furthermore

Table 13. CI results for the lowest states of the MeF_6^{2-} complexes. Energies (eV) given relative to the $^2T_{2g}$ (E_g'') state. Intramultiplet splittings (eV) given in parenthesis. **a** CoF_6^{2-}. **b** RhF_6^{2-}. **c** IrF_6^{2-}

State	Exp. [25]	Non-relativistic			Repr.	NR + SO	Relativistic			
		LFCI	CTCI	FOCI		SOCI[a]	LFCI(C)	LFCI(C+G)	CTCI	FOCI
$^2T_{2g}$	0	0.10	0.10	0.10	E_g''	0	0	0	0	0
					U_g'	0.15 (0.15)	0.14 (0.14)	0.14 (0.14)	0.14 (0.14)	0.14 (0.14)
					U_g'	0.32 (0)	0.28 (0)	0.27 (0)	0.41 (0)	0.49 (0)
					E_g''	0.39 (0.07)	0.33 (0.05)	0.31 (0.04)	0.43 (0.02)	0.51 (0.02)
$^4T_{1g}$	0.79	0.22	0.38	0.46	U_g'	0.38 (0.07)	0.33 (0.05)	0.31 (0.04)	0.43 (0.02)	0.51 (0.2)
					E_g'	0.35 (0.02)	0.31 (0.02)	0.29 (0.02)	0.43 (0.03)	0.52 (0.03)
					E_g'	1.26 (0)	1.25 (0)	1.24 (0)	1.22 (0)	1.28 (0)
					U_g'	1.27 (0.00)	1.25 (0.00)	1.24 (0.00)	1.22 (0.00)	1.28 (0.00)
$^4T_{2g}$	1.28	1.19	1.21	1.27	U_g'	1.31 (0.05)	1.26 (0.01)	1.25 (0.01)	1.24 (0.03)	1.31 (0.03)
					E_g''	1.33 (0.07)	1.26 (0.01)	1.26 (0.01)	1.26 (0.04)	1.32 (0.04)
$^6A_{1g}$	>0	−1.32	−0.50	−0.32	U_g'	−1.24 (0)	−1.29 (0)	−1.29 (0)	−0.53 (0)	−0.35 (0)
					E_g''	−1.24 (0.00)	−1.29 (0.00)	−1.29 (0.00)	−0.53 (0.00)	−0.35 (0.00)

[a] Spin–orbit parameter $\zeta_{3d} = 0.095$ eV was used in the perturbative SOCI calculations

Table 13b.

State	Exp. [26]	Non-relativistic			Repr.	NR+SO	Relativistic			
		LFCI	CTCI	FOCI		SOCI[a]	LFCI(C)	LFCI(C+G)	CTCI	FOCI
$^2T_{2g}$	0	0.21	0.21	0.21	E''_g	0	0	0	0	0
	<0.5				U'_g	0.34 (0.34)	0.32 (0.32)	0.31 (0.31)	0.31 (0.31)	0.31 (0.31)
					U'_g	1.57 (0)	1.58 (0)	1.59 (0)	1.72 (0)	1.71 (0)
					E''_g	1.62 (0.04)	1.62 (0.03)	1.62 (0.03)	1.76 (0.04)	1.74 (0.04)
$^4T_{1g}$	1.44	1.70	1.81	1.80	U'_g	1.82 (0.24)	1.76 (0.18)	1.75 (0.17)	1.85 (0.13)	1.84 (0.13)
					E'_g	1.87 (0.30)	1.80 (0.22)	1.79 (0.21)	1.89 (0.18)	1.88 (0.17)
					E'_g	2.51 (0)	2.48 (0)	2.48 (0)	2.50 (0)	2.46 (0)
					U'_g	2.53 (0.02)	2.50 (0.01)	2.49 (0.01)	2.52 (0.02)	2.48 (0.01)
$^4T_{2g}$	1.98	2.48	2.51	2.48	U'_g	2.63 (0.12)	2.53 (0.05)	2.52 (0.05)	2.57 (0.07)	2.53 (0.06)
					E''_g	2.66 (0.15)	2.54 (0.06)	2.53 (0.06)	2.58 (0.08)	2.55 (0.08)
$^6A_{1g}$		1.98	2.39	2.39	U'_g	2.23 (0)	2.12 (0)	2.10 (0)	2.43 (0)	2.43 (0)
					E''_g	2.25 (0.02)	2.13 (0.01)	2.11 (0.01)	2.44 (0.01)	2.44 (0.01)

[a] Spin–orbit parameter $\zeta_{4d}=0.209$ eV was used in the perturbative SOCI calculations

Table 13c.

State	Exp. [27, 28]	Non-relativistic			Repr.	NR + SO	Relativistic			
		LFCI	CTCI	FOCI		SOCI[a]	LFCI(C)	LFCI(C+G)	CTCI	FOCI
$^2T_{2g}$	0.00	0.60	0.60	0.60	E''_g	0	0	0	0	0
	0.82				U'_g	0.96 (0.96)	0.93 (0.93)	0.91 (0.91)	0.91 (0.91)	0.91 (0.91)
					U'_g	2.84 (0)	2.71 (0)	2.72 (0)	2.77 (0)	2.76 (0)
					E''_g	3.07 (0.23)	2.98 (0.27)	2.97 (0.26)	3.03 (0.27)	3.03 (0.26)
$^4T_{1g}$	2.45	2.99	3.06	3.05	U'_g	3.39 (0.55)	3.19 (0.48)	3.18 (0.46)	3.22 (0.46)	3.21 (0.46)
					E'_g	3.56 (0.72)	3.34 (0.63)	3.32 (0.61)	3.37 (0.60)	3.36 (0.60)
					E'_g	4.02 (0)	3.83 (0)	3.82 (0)	3.82 (0)	3.79 (0)
					U'_g	4.09 (0.07)	3.85 (0.02)	3.84 (0.02)	3.86 (0.04)	3.38 (0.04)
$^4T_{2g}$	3.09	3.74	3.77	3.74	E''_g	4.38 (0.36)	3.89 (0.06)	3.88 (0.06)	3.91 (0.09)	3.89 (0.10)
					U'_g	4.41 (0.39)	3.92 (0.08)	3.90 (0.08)	3.92 (0.10)	3.90 (0.11)
$^6A_{1g}$		4.19	4.21	4.20	U'_g	5.05 (0)	4.65 (0)	4.63 (0)		
					E''_g	5.05 (−0.01)	4.67 (0.03)	4.65 (0.02)		

[a] Spin–orbit parameter $\zeta_{5d} = 0.603$ eV was used in the perturbative SOCI calculations

Table 14. The absolute energies (Hartrees) of the $^2T_{2g}$ (E_g'') states. The energies contain a constant (spurious) contribution from the interactions between the point charges of the fitted potentials of Appendix 2. Note that the nuclei in the clusters are represented by a gaussian charge distribution with exponents 0.256207E+9, 0.176688E+9, 0.116194E+9 and 0.544946E+9 for Co, Rh, Ir and F respectively

	LFCI	SOCI	LFCI(C+G)	CTCI	FOCI
CoF_6^{2-} (NR)	−1992.199236	−1992.206122	—	−1992.255795	−1992.270679
CoF_6^{2-} (R)	−2003.456999	—	−2002.799990	−2003.509464	−2003.524783
RhF_6^{2-} (NR)	−5296.886858	−5296.897584	—	−5296.920006	−5296.923705
RhF_6^{2-} (R)	−5394.294470	—	−5390.801552	−5394.323816	−5394.327505
IrF_6^{2-} (NR)	−17416.517161	−17416.553167	—	−17416.539945	−17416.544430
IrF_6^{2-} (R)	−18456.812764	—	−18434.619602	−18456.829331	−18456.833325

neglected interaction with other d^5 states which may also decrease the spin–orbit splitting of the higher multiplets.

The effect of the inclusion of the Gaunt operator in the hamiltonian was studied perturbationwise at the LFCI level. We used the set of spinors that were determined at the Dirac–Coulomb level and thus neglected the effect of the Gaunt operator on the form of the spinors. The influence on the calculated splittings is small, giving as most significant result a decrease of the IrF_6^{2-} $^2T_{2g}$ spin–orbit splitting of 0.025 eV

6 Discussion

Experimentally all compounds are found to have a $^2T_{2g}$ low-spin ground state. Our calculations confirm this assignment except for CoF_6^{2-}, where the $^6A_{1g}$ state is found to be the lowest state. This discrepancy with experiment is at least partly due to the neglect of dynamical electron correlation that also lead to the discrepancies with experiment in the atomic calculations. The sextet state is described significantly better at the Hartree–Fock–LFCI level than the doublet or quartet states, because the Pauli correlation is incorporated whereas the Coulomb correlation is not, at this level of theory [24]. Miyoshi et al. [36] have published non-relativistic calculations on this system that support this assumption. In their LFCI calculations they find the ^6Al_g state lowest at 0.91 eV below the $^2T_{2g}$ state. When they incorporate a semi-empirical correction for the atomic correlation energies, employing the method of Pueyo and Richardson [37], they find the $^6A_{1g}$ state 0.12 eV above the $^2T_{2g}$ state.

An additional source of errors in the CoF_6^{2-} calculations is the uncertainty of 0.05 Å in the used experimental bond length. Variation of the bond length with 0.02 Å gives rise to variations in the calculated intermultiplet splittings of the order of 0.2 to 0.3 eV. Finally, the fact that we had to restrict the RAS3 space to include only a minimal number of virtuals will also contribute to the discrepancies.

For the Rh and Ir fluorides we cannot give an estimate of dynamical correlation effects on the basis of atomic results because no experimental spectra of Rh^{4+} and Ir^{4+} are available. It is, however, likely that dynamical correlation effects will also influence the spectrum of these compounds.

7 Conclusions

The excitation energies of the cobalt (IV), rhodium (IV) and iridium (IV) hexafluorides can be fairly well described by the CTCI–FOCI treatment outlined in Sect. 2.2. The electron–electron interaction dominates the spin–orbit coupling for all complexes, so the calculated states can be interpreted as (spin–orbit split) LS-coupled multiplets.

Calculated intermultiplet energy differences agree with experimental data to about 0.4 eV in CoF_6^{2-} and to about 0.8 eV in IrF_6^{2-}. For these energy differences, non-dynamical correlation effects that arise from low-lying charge transfer states are found to be most important in CoF_6^{2-}, while spin–orbit effects dominate in IrF_6^{2-}. The discrepancies with experiment can be explained by the influence of differential dynamical electron correlation effects that are largely neglected at the level of theory that we use here and to limitations in the RAS3 space that was used.

The intramultiplet spin–orbit splittings are not much influenced by correlation corrections. These splittings can be calculated to good accuracy in a ligand field CI calculation. Use of a perturbative model to calculate the spin–orbit coupling is also possible in these d^5 ions and gives good results for the CoF_6^{2-} and RhF_6^{2-} ions, but overestimates the splittings in the quartets of IrF_6^{2-}.

Acknowledgement. This investigation was supported by The Netherlands Foundations for Fundamental Research on Matter (FOM) with financial aid from The Netherlands Organisation for Scientific Research (NWO). Part of the calculations were performed on the National CRAY-YMP/464 supercomputer at SARA, Amsterdam, using a grant from the National Computing Facilities Foundation (NCF).

Appendix 1: Basis sets

Table A1.1. Exponents of the primitive gaussian functions

Cobalt		Rhodium		Iridium		Fluorine	
s	1084972.40	*s*	2731601.66	*s*	26668729.1	*s*	18648.5
s	162536.244	*s*	408859.481	*s*	3655468.76	*s*	2790.77
s	36991.6658	*s*	93307.3527	*s*	799486.001	*s*	633.258
s	10477.4164	*s*	26379.9304	*s*	223307.569	*s*	178.599
s	3418.40523	*s*	8563.26613	*s*	72755.38947	*s*	57.7896
s	1234.48863	*s*	3069.80285	*s*	26195.5709	*s*	20.4555
s	481.364201	*s*	1177.65743	*s*	10153.5021	*s*	7.58796
s	198.728746	*s*	472.694052	*s*	4066.33469	*s*	1.99213
s	20.7965155	*sd*	195.613241	*sd*	1660.71803	*s*	0.749854
s	0.145	*sd*	83.0173165	*sd*	695.762587	*s*	0.241845
sd	84.1211960	*sd*	35.8644033	*sd*	300.316974	*p*	63.1253
sd	25.1128635	*sd*	15.7285857	*sd*	131.207017	*p*	14.5012
sd	9.18340049	*sd*	6.92795231	*sd*	59.8738317	*p*	4.38233
sd	3.70926232	*sd*	3.01827958	*sd*	28.3242236	*p*	1.45355
sd	1.49235456	*sd*	1.19601332	*sd*	13.0883983	*p*	0.463237
sd	0.56778468	*sd*	0.44353579	*sd*	5.96839221	*p*	0.126578
sd	0.36051148	*sd*	0.18032814	*sd*	2.62206777	*d*	0.241845
p	2344.78030	*sd*	0.073	*sd*	1.06750738		
p	555.647128	*p*	54250.6937	*sd*	0.4219794		
p	178.863068	*p*	12847.3483	*sd*	0.13458954		
p	67.1082327	*p*	3042.43775	*sd*	0.0429		
p	27.3476842	*p*	986.433555	*p*	630825.605		
p	11.6614996	*p*	375.207531	*p*	150637.678		
p	4.77240079	*p*	157.689216	*p*	35971.4473		
p	1.99067313	*p*	70.4823506	*p*	8589.78338		
pf	0.79864849	*p*	32.7196868	*p*	2791.38561		
p	0.32	*p*	14.6128764	*p*	1066.37478		
		p	6.75523649	*p*	446.084374		
		p	3.06574636	*pf*	161.628290		
		p	1.34905790	*pf*	58.0553565		
		pf	0.56425188	*pf*	25.2728514		
		p	0.236	*pf*	11.3439089		
				pf	4.89293799		
				pf	1.85277206		
				pf	0.78292625		
				p	0.27559172		

Appendix 2: Fitted madelung potentials

Table A2.1. Potential (V) of the Cs_2CoF_6 lattice

Atom	Position in lattice coordinates	Number of equivalent positions	Formal charge	Fit charge	Distance to central Co (Å)
Co	(0.00, 0.00, 0.00)	1	4+	In cluster	0.0
F	(0.20, 0.00, 0.00)	6	1−	In cluster	1.73
Cs	(0.25, 0.25, 0.25)	8	1+	0.9812	3.86
F	(0.50, 0.30, 0.00)	24	1−	−0.7679	5.22
Co	(0.50, 0.50, 0.00)	12	4+	1.9598	6.30
F	(0.80, ,0.00, 0.00)	24	1−	1.1527	7.18
Cs	(0.75, 0.25, 0.25)	24	1+	−0.7872	7.39

Table A2.2. Potential (V) of the Cs_2GeF_6 lattice

Atom	Position in lattice coordinates	Number of equivalent positions	Formal charge	Fit charge	Distance to central Ge (Å)
Ge (Rh, Ir)	(0.00, 0.00, 0.00)	1	4+	In cluster	0.0
F	(0.20, 0.00, 0.00)	6	1−	In cluster	
Cs	(0.25, 0.25, 0.25)	8	1+	0.9811	3.91
F	(0.50, 0.30, 0.00)	24	1−	−0.7718	5.26
Ge	(0.50, 0.50, 0.00)	12	4+	2.0358	6.38
F	(0.80, 0.00, 0.00)	24	1−	1.1269	7.22
Cs	(0.75, 0.25, 0.25)	24	1+	−0.8195	7.48

Table A2.3. Accuracy (V) of the point charge fits of the Madelung potential

Crystal	maximum error	average error
Cs_2CoF_6	0.0025	0.00004
Cs_2GeF_6	0.0024	0.00004

References

1. Visser O, Visscher L, Aerts PJC, Nieuwpoort WC (1992) Theor Chim Acta 81:405
2. Visser O, Visscher L, Aerts PJC, Nieuwpoort WC (1992) J Chem Phys 96:2910
3. Visscher L, Saue T, Nieuwpoort WC, Faegri K, Gropen O (1993) J Chem Phys 99:6704
4. Visscher L, Visser O, Aerts PJC, Merenga H, Nieuwpoort WC (1994) accepted for publication in Comp Phys Comm
5. Moss RE (1968) Advanced molecular quantum mechanics. Benjamin, London
6. Rose ME (1961) Relativistic electron theory. Wiley, New York
7. Breit G (1929) Phys Rev 34:553
8. Kim YK (1967) Phys Rev 154:17
9. Gaunt JA (1929) Proc R Soc A 122:513

10. Roothaan CCJ (1960) Rev Mod Phys 32:179
11. Visscher L, Aerts PJC, Visser O (1991) General contraction in four-component relativistic Hartree–Fock calculations. In: Wilson, Grant, Gyorffy (eds) The effects of relativity in atoms, molecules and the solid state. Plenum, New York, pp 197–205
12. Olsen J, Roos BO, Jørgensen P, Jensen HJAa (1988) J Chem Phys 89:2185
13. Davidson ER (1975) J Comput Phys 17:87
14. Janssen GJM, Nieuwpoort WCN (1988) Phys Rev B 38:3449
15. Janssen GJM, Nieuwpoort WCN (1988) Int J Quant Chem Symp 22:679
16. ASCF: Atomic Self Consistent Field code, developed by the theoretical chemistry group in Groningen.
17. Wachters AJH (1971) Ph.D. Thesis, University of Groningen
18. Dyall KG, Grant IP, Johnson CT, Plummer EP, Parpia F (1988), Computer Phys Commun 50:375
19. Sugar J, Corliss C (1981) J Phys Chem Ref Data 101:1097
20. Moore CE (1958) Circular of the National Bureau of Standards 467:181
21. Condon EU, Shortley GH (1953) The theory of atomic spectra. Cambridge University Press, London
22. Griffith JS (1971) The theory of transition metal ions. Cambridge University Press, London
23. Nieuwpoort WC (1978) Calculations on the electronic states of transition metal and rare-earth compounds. In: Roos B, Diercksen GHF (eds) Proceedings of the 4th Seminar on Computational Methods in Quantum Chemistry. Orenäs
24. Vanquickenborne LG, Henderickx M, Postelmans D, Hyla-Krispin I, Pierloot K (1988) Inorg Chem 27:900
25. Allen GC, Warren KD (1969) Inorg Chem 8:1902
26. Allen GC, El-Sharkawy GAM, Warren KD (1973) Inorg Chem 10:2231
27. Allen GC, Al-Mobarak R, El-Sharkawy GAM, Warren KD (1972) Inorg Chem 11:787
28. Weiss LC, McCarthy PJ, Jainski JP, Schatz PN (1978) Inorg Chem 17:2689
29. Quail JW, Rivett GA (1972) Can J Chem 50:2447
30. Brisdon AK, Holloway J, Hope EG, Levason W, Ogden JS Saad AK (1992) J Chem Soc Dalton Trans 447
31. Brisdon AK, Holloway J, Hope EG, Levason W, Ogden JS, Saad AK (1992) J Chem Soc Dalton Trans 139
32. Miyoshi E, Kashiwagi H (1983) Int J Quant Chem 24:85
33. Mulliken R (1955) J Chem Phys 23:1833
34. Ballhausen CJ (1962) Introduction to ligand field theory. McGraw-Hill, New York, pp 118–119
35. See reference 22, p 421
36. Miyoshi E, Takada T, Obara S, Kashiwagi H, Ohno K (1981) Int J Quant Chem 19:451
37. Pueyo L, Richardson JW (1977) J Chem Phys 67:3577